Chemistry Europe
European Chemical Societies Publishing

WILEY VCH

Excellence in Chemistry Research

Announcing our new flagship journal

- Gold Open Access
- Publishing charges waived
- Preprints welcome
- Edited by active scientists

Meet the Editors of *ChemistryEurope*

Luisa De Cola
Università degli Studi di Milano Statale, Italy

Ive Hermans
University of Wisconsin-Madison, USA

Ken Tanaka
Tokyo Institute of Technology, Japan

Chemistry–A European Journal
Research Article
doi.org/10.1002/chem.202203798
Chemistry Europe
European Chemical Societies Publishing
www.chemeurj.org

AAZTA-Like Ligands Bearing Phenolate Arms as Efficient Chelators for ^{68}Ga Labelling in vitro and in vivo

Jonathan Martinelli,[a] Leonardo Maria Zapelli,[a] Mariangela Boccalon,[b] Adrienn Vágner,[c] Gábor Nagy,[c] Anikó Fekete,[d] Dezső Szikra,[d] György Trencsényi,[d] Zsolt Baranyai,*[b] and Lorenzo Tei*[a]

Abstract: The introduction of a phenolate pendant arm in place of an acetate on AAZTA- and DATA-like ligands resulted in hepta- and hexadentate chelators able to form Ga(III) complexes with thermodynamic stability and kinetic inertness higher than that of other Ga(III) complexes based on the parent 6-amino-6-methylperhydro-1,4-diazepine scaffold. In particular, the heptadentate AAZ3A-endoHB with a phenolate arm on an endocyclic N-atom shows a logK_{GaL} of 27.35 and a remarkable resistance to hydroxide coordination up to basic pH (pH > 9). This behaviour allows to also improve the kinetic inertness of the complex showing a dissociation half-life ($t_{1/2}$) at pH 7.4 of 76 h. Although also the hexadentate AAZ2A-exoHB chelator forms a stable (logK_{GaL} = 24.69) and inert ($t_{1/2}$ = 33 h at pH 7.4) Ga(III) complex, the ^{68}Ga labelling showed a better radiochemical yield with AAZ3A-endoHB, especially at room temperature. Thus, a bifunctional chelator of AAZ3A-endoHB was synthesized bearing an isothiocyanate group that was conjugated to the N-terminus of a c(RGD) peptide for integrin receptor targeting. Finally, the conjugate was successfully labelled with ^{68}Ga isotope, and the resulting radiotracer tested for its stability in human serum and then in vivo for targeting B16-F10 tumours with miniPET imaging.

Introduction

Positron emission tomography (PET) is a diagnostic technique that nowadays is routinely applied in hospitals for medical purposes. It is based on the use of radiotracers, that is, chemical compounds containing radioactive isotopes able to emit β^+ particles that annihilate after a short path (mm) with consequent emission of two γ rays. This high-energy radiation is finally detected by an instrument that allows mapping the distribution of the radiotracer through the body of the patient. The isotopes that can be exploited for PET technique must then satisfy some specific requirements such as the decay modality (β^+-emitters), the half-life and their availability. Alongside fluorine-18, mostly introduced onto bioactive molecules by covalent bonding as in ^{18}F-FDG[1] (although some procedures have been recently developed to include it as fluoranylaluminum ion [Al^{18}F]$^{2+}$ chelated by suitable ligands),[2,3] gallium-68 is a very common choice in PET applications.[4,5] It can be easily produced on-site via a ^{68}Ge/^{68}Ga generator system; it has a relatively short half-life ($t_{1/2}$ = 67.71 min) after which it decays to stable ^{68}Zn; its emitted positron annihilates with emission of two γ-rays whose energy is in the ideal range of applicability (E_β^{max} = 1.89 MeV, 89% decays through positron emission).

The exceptional diagnostic potential of PET and the increasing availability of novel receptor-specific peptides and high affinity targeting vectors have led to the design and testing of a large number of ^{68}Ga-based radiopharmaceuticals in oncology, cardiology, neurology, and infectious diseases for a personalized medical approach.[6,7] Among these, ^{68}Ga tracers based on prostate specific membrane antigen (PSMA) inhibitors[8,9] and somatostatin analogues[10,11] have firmly established ^{68}Ga in clinical nuclear medicine allowing accurate quantitative diagnoses and staging for subsequent selection and planning of therapeutic methods.

Gallium(III) coordination compounds can be tetra-, hexa- or hepta-coordinated and must be stably chelated by a polydentate ligand. The relatively short half-life implies that the complexation has to take place quickly and, in case of conjugation to a sensitive bioactive molecule as targeting vector, harsh conditions in terms of temperature and pH must be avoided. Moreover, in addition to a high affinity and

[a] Dr. J. Martinelli, L. M. Zapelli, Prof. Dr. L. Tei
Department of Science and Technological Innovation
Università del Piemonte Orientale
Viale Michel 11, 15121 Alessandria (Italy)
E-mail: lorenzo.tei@uniupo.it
[b] Dr. M. Boccalon, Dr. Z. Baranyai
Bracco Research Centre
Bracco Imaging S.p.A.
Via Ribes 5, 10010 Colleretto Giacosa (Italy)
E-mail: zsolt.baranyai@bracco.com
[c] Dr. A. Vágner, Dr. G. Nagy
Scanomed Ltd.
Nagyerdei krt. 98, 4032 Debrecen (Hungary)
[d] Dr. A. Fekete, Dr. D. Szikra, Dr. G. Trencsényi
Division of Nuclear Medicine and Translational Imaging
Department of Medical Imaging, Faculty of Medicine
University of Debrecen
Nagyerdei krt. 98, 4032 Debrecen (Hungary)

Supporting information for this article is available on the WWW under https://doi.org/10.1002/chem.202203798

selectivity for Ga(III), the chelate should possess high kinetic inertness to avoid dissociation in the biofluids before excretion and/or radioactive decay.[12,13] So far, several chelators have been proposed for ^{68}Ga labelling and conjugation to targeting vectors for molecular imaging PET applications. These chelators can be divided into three main classes: i) linear structures, among which HBED (*N,N'*-bis(2-hydroxybenzyl)ethylenediamine -*N,N'*-diacetic acid)[14] and CHXdedpa (CHX = cyclohexane, dedpa = 1,2-[[6-carboxy-pyridin-2-yl]-methylamino]ethane)[15] are the most used; ii) macrocyclic ligands belonging to the family of DOTA (1,4,7,10-tetraazacyclododecane tetraacetic acid)[16–18] and NOTA (1,4,7-triazacyclononane-1,4,7-triacetic acid)[19] analogues, iii) mesocyclic chelators such as AAZTA (6-amino-6-methylperhydro-1,4-diazepine tetraacetic acid)[20] and derivatives[21,22] (Figure 1).

One of the advantages of the AAZTA-like family is the intermediate characteristics of the chelator which is in between the linear and macrocyclic structure allowing both fast complexation kinetics and high kinetic inertness of the Ga(III) complex. To this end, bifunctional derivatives of AAZTA were used for conjugation to peptides (PSMA, RGD, minigastrin) showing accumulation in tumours of the corresponding $^{68}Ga^{3+}$ chelates.[21,23–26] Modifications of the AAZTA structure were designed to obtain more rigid backbones such as in CyAAZTA[27,28] and PIDAZTA[29] (Figure 1), and thus more inert Ga(III) complexes, or to lower the denticity obtaining the hexadentate DATA ligands (Figure 1) to allow a better match with the hexacoordinate Ga(III) ion.[20] DATA^m bifunctional derivatives were also conjugated to targeting vectors such as PSMA[30] or fibroblast activation protein inhibitor (FAP)[31] for tumour imaging. However, the success of AAZTA and derivatives is weakened by the formation of a hydroxo-species at physiological pH that sometimes accelerates the metal dissociation rate as well as worsening radiolabelling performance. In fact, except the case of [Ga(PIDAZTA 4aR*,10aR*)OH]$^-$ which presents an exceptionally high kinetic inertness albeit in the form of the hydroxo-complex, the other GaAAZTA-like complexes have lower kinetic inertness ($t_{1/2}$ 0.3–21 h at pH 7.4) due to the instability of the hydroxo-complex, the dominant species at physiological pH.

We have recently introduced phenolate donors on the amino nitrogen atoms of the 6-amino-6-methyl-1,4-diazepine scaffold in order to increase contemporaneously both the basicity and the rigidity of the ligand and increase both the stability and the kinetic inertness of the corresponding metal complexes.[32,33] In this context, two regioisomeric AAZ3A-ligands bearing a hydroxybenzyl pendant arm on the exocyclic or endocyclic (i.e., AAZ3A-endoHB, Figure 1) nitrogen atoms have been recently reported to form Gd(III) complexes with completely different structures, hydration numbers, stabilities and dissociation kinetics, highlighting the importance of ligand topology in metal ion coordination properties.[32] Considering that there are not many examples of ^{68}Ga-chelators having phenolate donors,[34–38] with the main exception of HBED, we decided to undertake a study on the thermodynamic stability and kinetic inertness of the Ga(III) and ^{68}Ga-radiolabelled complexes of two chelators bearing hydroxybenzyl arms: one heptadentate, AAZ3A-endoHB and one hexadentate, AAZ2A-exoHB. Subsequently, the chelator with the best performance was chosen and a bifunctional derivative was synthesized for the conjugation to a cyclo(RGD) peptide for $\alpha_v\beta_3$ integrin targeting and a preliminary in vivo test was performed.

Results and Discussion

Solution equilibrium properties of Ga(III) complexes

The syntheses of the two ligands AAZ2A-exoHB and AAZ3A-endoHB have been recently described by our group.[32,33] It should be highlighted that the targeted PET applications require high thermodynamic stability and kinetic inertness of

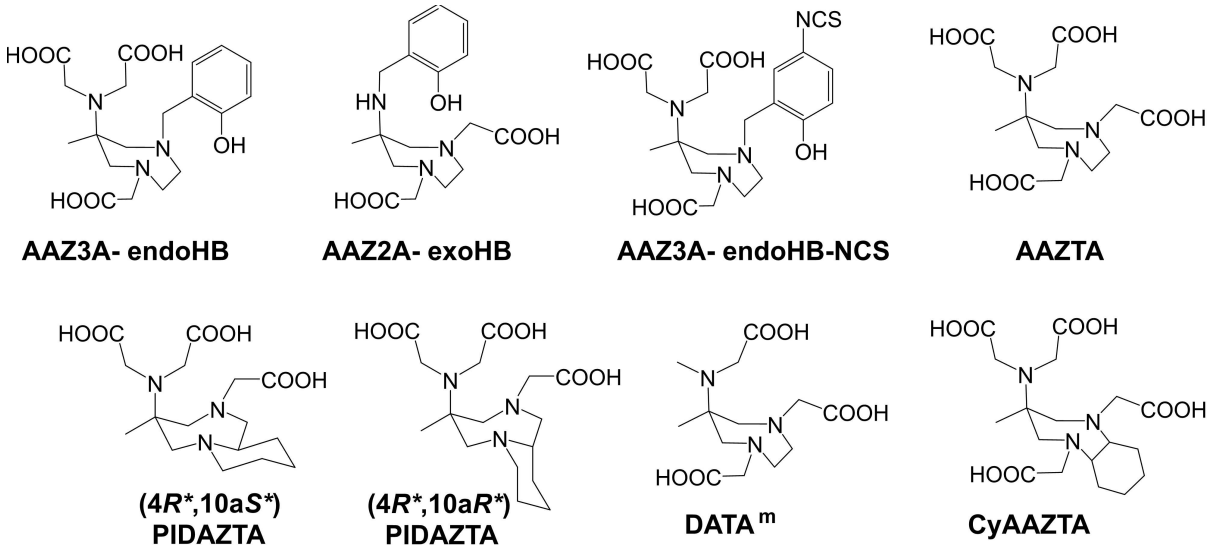

Figure 1. Structures of the ligands reported in this paper and other mentioned AAZTA-derivatives.

the ^{68}Ga(III) complexes to minimize the in vivo transmetallation or transchelation reactions with the potential endogenous competition partners.[39–42] Considering the high conditional stability and the dominance of the $[Ga(OH)_4]^-$ species at high pH values (pH > 6), the stability constants of the Ga(III) complexes have been often determined by following the competition reaction for the Ga^{3+} ion between the ligand and OH^- with pH-potentiometry and multinuclear NMR spectroscopy.[39,43–45]

Thus, the stability and protonation constants of [Ga(AAZ3A-endoHB)]$^-$ and [Ga(AAZ2A-exoHB)] were calculated by using the data obtained with pH-potentiometry and ^{1}H and ^{71}Ga NMR spectroscopy. ^{1}H and ^{71}Ga NMR spectra of the Ga(III) – AAZ3A-endoHB and Ga(III) – AAZ2A-exoHB systems at different pH values are reported in Figures S2–S5. The stepwise protonation constants of the free AAZ3A-endoHB and AAZ2A-exoHB ligands ($\log K_i^H$), obtained in our previous[32] and present works, were used for the calculation of the stability and the protonation constants of [Ga(AAZ3A-endoHB)]$^-$ and [Ga(AAZ2A-exoHB)] (AAZ2A-exoHB: $\log K_1^H = 11.42(1)$, $\log K_2^H = 8.96(2)$, $\log K_3^H = 5.46(3)$, $\log K_4^H = 3.37(3)$ and $\log K_5^H = 0.85(4)$; AAZ3A-endoHB: $\log K_1^H = 11.47$, $\log K_2^H = 9.18$, $\log K_3^H = 6.17$, $\log K_4^H = 3.76$, $\log K_5^H = 2.69$ and $\log K_6^H = 1.43$, 25 °C, 0.15 M NaCl).[32] The experimental details, the definitions and equations used for the evaluation of the equilibrium data and the equilibrium characterization of Ca(II)-, Zn(II)-, Cu(II)- and Ga(III) complexes formed with AAZ3A-endoHB and AAZ2A-exoHB are reported in Supporting Information.

As shown in Table 1, the $\log K_{GaL}$ value of [Ga(AAZ3A-endoHB)]$^-$is higher by 6–8 log*K* units than that of the Ga(III) complexes with PIDAZTA, DATA^m, CyAAZTA and AAZTA, explained by the higher basicity of the phenolate donor and consequently by the higher total basicity of AAZ3A-endoHB ($\Sigma \log K_i^H$). On the other hand, [Ga(AAZ2A-exoHB)] shows a $\log K_{GaL}$ value about 3 orders of magnitude lower than [Ga-(AAZ3A-endoHB)]$^-$ due to the lack of one carboxylate donor and to the higher basicity of the ring-N donor atoms in the AAZ3A-endoHB ligand. The stability constant of [Ga(AAZ2A-exoHB)] is higher than that reported for all the other complexes listed in Table 1 thanks to the coordination of the basic phenolate donor to the Ga(III) ion. In the Ga(III) complexes with AAZTA-like ligands the Ga(III) ion is typically coordinated by three amino-N and three carboxylate-O$^-$ donor atoms.[28,29,39,46] In the complexes reported in this work the Ga(III) ion is presumably coordinated by 3 amino-N, two carboxylate-O$^-$ and the very basic phenolate-O$^-$ donor atoms which can be responsible for the much higher stability constants of both complexes with respect to those of the Ga(III) complexes with PIDAZTA, DATA^m, CyAAZTA and AAZTA. Interestingly, the formation of [Ga(AAZ3A-endoHB)OH]$^{2-}$ species ($\log K_{Ga(L)OH}$, Table 1) occurs at remarkably higher pH values than that of [Ga(AAZ2A-exoHB)H_{-1}]$^-$, [Ga(PIDAZTA)H_{-1}]$^-$, [Ga(AAZTA)H_{-1}]$^{2-}$, [Ga(DATA^{5m})H_{-1}]$^-$ and [Ga(CyAAZTA)H_{-1}]$^{2-}$. Presumably, the formation of the [Ga(L)H_{-1}]$^{2-}$ species takes place by the substitution of one carboxylate donor atom with the OH^- ion in the inner-sphere of the Ga(III) ion. However, the negative charge of the [Ga(AAZ3A-endoHB)]$^-$ complex and the coordination of the very basic and bulky phenolate-O$^-$ can hinder the entrance of the OH^- ion to the inner-sphere of Ga(III). A comparison between the $\log \beta_{Ga(L)OH}$ values of the [Ga(L)H_{-1}] species (Table 1) shows that [Ga(AAZ2A-exoHB)H_{-1}]$^-$ has the highest cumulative stability constant among the Ga(III) complexes formed with AAZTA derivatives. The equilibrium data obtained by pH-potentiometry and multinuclear NMR spectroscopy were used to calculate the species distribution diagram for the Ga(III) – AAZ3A-endoHB and AAZ2A-exoHB systems (Figure 2). The amount of $[Ga(OH)_4]^-$ species determined by ^{71}Ga NMR studies are also shown in Figure 2. The species distribution diagrams, and the ^{1}H and ^{71}Ga NMR spectra (Figures 2, S2–S5) indicate that the [Ga(AAZ3A-endoHB)]$^-$ and [Ga(AAZ2A-exoHB)] complex formation occurs at pH ≥ 2.0. The deprotonation of the [Ga(HL)] and $[Ga(H_2L)]^+$ species results in a slight upfield shift of the CH_2-protons in the ^{1}H NMR signals, whereas the chemical shifts of the aryl protons are unchanged in the pH range 2–3. By taking into account the upfield shift of the CH_2-protons, the protonation of [Ga(AAZ2A-exoHB)] and [Ga(AAZ3A-endoHB)]$^-$ takes place at the weakly and/or non-coordinated carboxylate group of the ligand. In the pH range 3.0–5.0 and 3.5–9.5, the complexes [Ga(AAZ2A-exoHB)] and [Ga(AAZ3A-endoHB)]$^-$ dominate, as clearly indicated by the unchanged ^{1}H NMR spectra of the Ga(III) – AAZ2A-exoHB and Ga(III) – AAZ3A-endoHB systems (Figures S2 and S4). The chemical shifts and the linewidth of the ^{71}Ga NMR signals are strongly influenced by the nature of the donor atoms and by the symmetry of the Ga(III) complexes ([Ga(DATA^m)]: $\delta_{Ga} = 129$ ppm, $\nu_{1/2} = 1000$ Hz; [Ga(CyAAZTA)]$^-$: $\delta_{Ga} = 119$ ppm, $\nu_{1/2} = 4700$ Hz, 308 K and [Ga(AAZTA)]$^-$: $\delta_{Ga} = 118$ ppm, $\nu_{1/2} = 2200$ Hz).[28,34,39,46] On the other hand, the linewidth of the ^{71}Ga NMR signal could be influenced by the

Table 1. Stability and protonation constants at 25 °C of Ga(III) complexes of AAZ3A-endoHB and AAZ2A-exo-HB compared to the Ga(III) complexes with similar ligands (PIDAZTA, DATA^m, CyAAZTA, AAZTA and NOTA).

	I	GaL	Ga(HL)	Ga(H_2L)	Ga(L)H_{-1}	$\log \beta_{Ga(L)H-1}$	pGa[a]
[Ga(AAZ3A-endoHB)]	0.15 M NaCl	27.35 (1)	3.89 (3)	2.45 (2)	9.96 (2)	17.39 (2)	22.42
[Ga(AAZ2A-exoHB)]	0.15 M NaCl	24.69 (9)	2.60 (2)	–	6.44 (1)	18.24 (9)	21.05
[Ga(PIDAZTA 4aR*, 10aS*)][29]	0.15 M NaCl	18.77	2.41	–	4.04	14.74	20.08
[Ga(PIDAZTA 4aR*, 10aR*)][29]	0.15 M NaCl	21.70	2.51	–	3.75	17.94	21.74
[Ga(DATA^m)][46]	0.15 M NaCl	21.54	2.42	–	6.25	15.29	20.15
[Ga(CyAAZTA)]$^-$[28]	0.1 M KCl	21.39	4.09	2.32	7.31	14.08	20.65
[Ga(AAZTA)]$^-$[39]	0.15 M NaCl	21.15	3.14	1.14	4.60	16.57	22.17
[Ga(NOTA)][49]	0.1 M TMACl	29.60	0.9	–	9.83	19.77	24.77

[a] $pGa = -\log[Ga^{3+}]_{free}$, $[Ga^{3+}]_t = 1$ μM, $[L]_t = 10$ μM, pH = 7.4.[48]

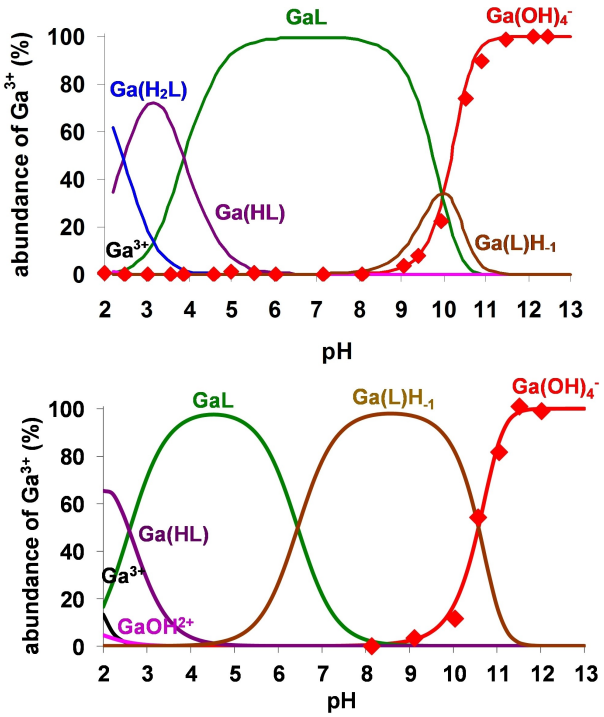

Figure 2. Species distribution and amount of $[Ga(OH)_4]^-$ (◆) calculated from the ^{71}Ga NMR studies of Ga^{3+}-AAZ3A-endoHB (*top*) and Ga^{3+}-AAZ2A-endoHB (*bottom*) systems. $[Ga^{3+}]$ = [AAZ3A-endoHB] = 2.25 mM; [AAZ2A-exoHB] = 2.5 mM, 0.15 M NaCl, 25 °C.

interaction of the nuclear quadrupolar moment with the electric-field gradient at the ^{71}Ga nucleus.[47] In this respect, the ^{71}Ga NMR signals of [Ga(AAZ2A-exoHB)] and $[Ga(AAZ3A\text{-}endoHB)]^-$ are very broad probably due to the asymmetric coordination environment of the Ga(III) ion (Figures S3 and S5).

Since the ^{1}H NMR spectra of [Ga(AAZ2A-exoHB)] contain several sharp multiplets (Figure S4), it can be assumed that such complex has a rigid structure with Ga(III) tightly coordinated by the N_3O_3 donor atoms set. On the contrary, the ^{1}H NMR spectra of $[Ga(AAZ3A\text{-}endoHB)]^-$ show several broad multiplets (Figure S2) probably because, besides the N_3O_3 donor set coordinated to Ga(III), one of the acetate pendant arm does not participate in the coordination of the metal ion. Comparing these results with literature data, it is possible to conclude that Ga(III) complexes with hexadentate AAZTA-like ligands, such as [Ga(AAZ2A-exoHB)] and $[Ga(DATA^m)]$,[46] are more rigid and the ^{1}H NMR spectra are sharper than those with heptadentate ligands such as $[Ga(AAZ3A\text{-}endoHB)]^-$ and $[Ga(AAZTA)]^-$.[39] In the latter complexes, conformational motions of the diazepine ring and the pendant arms should be responsible of the broadening of the ^{1}H NMR signals.

The formation of the $[Ga(L)H_{-1}]^-$ species via the substitution of one carboxylate-O^- with the OH^- ion in [Ga(AAZ2A-exoHB)] results in the upfield shift of CH_2- and CH_3-protons ^{1}H NMR signals, whilst the chemical shifts of the aryl protons are unchanged in the pH range 5.0–9.0 (Figure S4). At pH > 9.5, the competition of AAZ2A-exoHB and AAZ3A-endoHB with OH^- ion for Ga^{3+} is highlighted by the appearance of the ^{71}Ga NMR signal of $[Ga(OH)_4]^-$ (δ_{Ga} = 223 ppm, $\nu_{1/2}$ = 85 Hz, Figures S3 and S5) and of the ^{1}H NMR signals of the free AAZ2A-exoHB and AAZ3A-endoHB ligands (Figures S2 and S4). Interestingly, the formation of $[Ga(AAZ3A\text{-}endoHB)H_{-1}]^{2-}$ causes a slight upfield shift of CH_2-protons ^{1}H NMR signals, whereas the chemical shifts of the aryl protons are unchanged, which confirms the substitution of one carboxylate-O^- donor by OH^-. The intensity of the ^{71}Ga NMR signal of $[Ga(OH)_4]^-$ increases by increasing pH due to the dissociation of $[GaL]^-$ and $[Ga(L)H_{-1}]$ species in the pH ranges 9.5–11.0. The ^{1}H NMR signal of the CH_3-protons of free and complexed AAZ2A-exoHB and AAZ3A-endoHB are well separated with chemical shifts of 0.8 and 1.2 ppm, respectively. Thus, the formation of free AAZ2A-exoHB and AAZ3A-endoHB ligands results in a significant upfield shift of CH_3-protons ^{1}H NMR signal, whereas the resonance of CH_3-protons in [Ga(AAZ2A-exoHB)] and $[Ga(AAZ3A\text{-}endoHB)]^-$ remains unchanged. The integral values of the CH_3-protons signals of the Ga(III) complex decreases with increasing the pH above 10 due to the dissociation of the Ga(III) complex and the formation of $[Ga(OH)_4]^-$ (Figures S2 and S4).

Dissociation kinetics of Ga^{3+} complexes

For the targeted application of ^{68}Ga based radiodiagnostics in PET imaging, their kinetic inertness must be evaluated in order to guarantee the delivery of the radioisotope in the form of intact complex to the target organ or tissue. The Ga(III) complexes are generally characterized by relatively high thermodynamic stability. However, the large excess of the possible competition partners in body fluids, i.e., endogenous metal ions and ligands, may result in competition reactions (transmetallations or transchelations) with the administered ^{68}Ga(III) complexes. The extent of the competition reactions after in vivo administration of a ^{68}Ga(III) complex is determined by thermodynamic relations, expressed by the stability constants of the different complexes formed in body fluids. Based on the equilibrium data (Tables 1 and S1), the endogenous metal ions (mainly Cu(II) and Zn(II)) or serum proteins such as transferrin may compete with [Ga(AAZ2A-exoHB)] and $[Ga(AAZ3A\text{-}endoHB)]^-$ resulting in the release of the Ga^{3+} ion. The kinetic properties of Ga(III) complexes is often measured in strong acidic ($[H^+] > 1.0$ M) and basic ($[OH^-] > 0.1$ M) conditions.[40,47,49] In this study, the kinetic inertness was determined via spectrophotometry by investigating the transmetallation reactions of [Ga(AAZ2A-exoHB)] and $[Ga(AAZ3A\text{-}endoHB)]^-$ with Cu^{2+} in the pH ranges 2.8–4.5 and 8.5–10.5, with 10 and 20 fold Cu^{2+} excess and in the presence of citrate to prevent the hydrolysis of the released Ga^{3+} and the exchanging Cu^{2+} ions. The k_d pseudo-first-order rate constants characterizing the transmetallation reactions of [Ga(AAZ2A-exoHB)] and $[Ga(AAZ3A\text{-}endoHB)]^-$ (Figure S8) indicate that the rate of the transmetallation reaction is directly proportional to the concentration of H^+ and OH^- but it does not depend on $[Cu^{2+}]$. Accordingly, the reactions occur through the spontaneous (k_0), proton (k_1) and OH^--ion assisted ($k_{GaLH\text{-}1}$ and k_{OH}) dissociation of Ga(III) complexes, followed by a fast reaction

between the released AAZ2A-exoHB and AAZ3A-endoHB ligands and the free Cu^{2+} ions. The mechanisms of the transmetallation reactions for both Ga(III) complexes are summarized in Scheme 1. The rate and protonation constants characterising the transmetallation reaction of [Ga(AAZ2A-exoHB)] and [Ga(AAZ3A-endoHB)]$^-$ with Cu^{2+} are listed and compared with those of [Ga(PIDAZTA)], [Ga(DATA^m)], [Ga-(CyAAZTA)]$^-$ and [Ga(AAZTA)]$^-$ complexes in Table 2. Experimental details, definitions and equations used for the evaluation of the kinetic data are summarized in the Supporting Information. According to the kinetic data, the obtained k_0 values are very low and the error in them is very high, indicating the unimportance of the spontaneous dissociation for [Ga(AAZ2A-exoHB)] and [Ga(AAZ3A-endoHB)]$^-$.

The k_{GaLH-1} rate constant characterizes the spontaneous dissociation of [Ga(AAZ3A-endoHB)H_{-1}]$^-$, similar to that of [Ga(PIDAZTA 4aR*,10aS*)H_{-1}]$^-$ and about 1–3 orders of magnitude higher than that of [Ga(AAZ2A-exoHB)H_{-1}]$^-$, [Ga(PIDAZTA 4aR*,10aR*)H_{-1}]$^-$, [Ga(DATA^m)H_{-1}]$^-$, [Ga(CyAAZTA)H_{-1}]$^{2-}$ and [Ga-(AAZTA)H_{-1}]$^{2-}$ complexes.

The spontaneous dissociation of the [Ga(L)H_{-1}] species presumably occurs by the intramolecular rearrangement of the Ga(III) complex and by the stepwise de-coordination of each donor atom and consequent release of the Ga^{3+} ion. The relatively fast spontaneous dissociation of [Ga(AAZ3A-endoHB)H_{-1}]$^{2-}$ can be ascribed to the less rigid and unfavourable coordination environment for the Ga(III) ion provided by 3 amino-N, carboxylate- and phenolate-O$^-$ donor atoms and the OH^- ion leading to faster intramolecular rearrangements and dissociation processes.

However, the spontaneous dissociation of the [Ga(L)H_{-1}]$^-$ species has a substantial contribution to the dissociation of [Ga(AAZ3A-endoHB)]$^-$ at higher pH values (pH > 9, Figure S8) due to the relatively high protonation constant of the [Ga-(AAZ3A-endoHB)H_{-1}]$^{2-}$ species (Table 1). The transmetallation of [Ga(AAZ2A-exoHB)] can also take place by the OH^--assisted dissociation (k_{OH}) of the [Ga(L)H_{-1}] species that dominates at pH ≥ 7.5 (Figure 2). The k_{OH} rate constant of [Ga(AAZ2A-exoHB)] is about 3, 10 and 20 times lower than those of [Ga(AAZTA)]$^-$, [Ga(DATA^m)] and [Ga(CyAAZTA)]$^-$ complexes respectively, due to the strong interaction between the coordinated phenolate-O$^-$ donor atom and Ga(III). By considering the rate and equilibrium constants presented in Table 2, the half-lives ($t_{1/2} = \ln 2/k_d$) of the dissociation reactions of [Ga(AAZ2A-exoHB)] and [Ga(AAZ3A-endoHB)]$^-$ close to physiological conditions (pH = 7.4, 25 °C) were calculated and compared with those of other Ga(III) complexes with AAZTA-like ligands. The dissociation half-life of [Ga(AAZ2A-exoHB)] is about 2.5 times lower than [Ga(AAZ3A-endoHB)]$^-$ due to the dominance of the hydroxo [Ga(AAZ2A-exoHB)H_{-1}] species at pH 7.4. The $t_{1/2}$ value of [Ga(AAZ3A-endoHB)]$^-$ is about 4 times smaller than that of [Ga(PIDAZTA 4aR*,10aR*)], and about 30, 7, 9 and 3.5 times higher than the dissociation half-life of [Ga(PIDAZTA 4aR*,10aS*)], [Ga(DATA^m)], [Ga(CyAAZTA)]$^-$ and [Ga(AAZTA)]$^-$, respectively, highlighting that the substitution of one carboxylate with one phenolate pendant arm in the AAZTA ligand results in a highly inert Ga(III) complex, due to a small contribution of the OH^--assisted dissociation at physiological conditions.

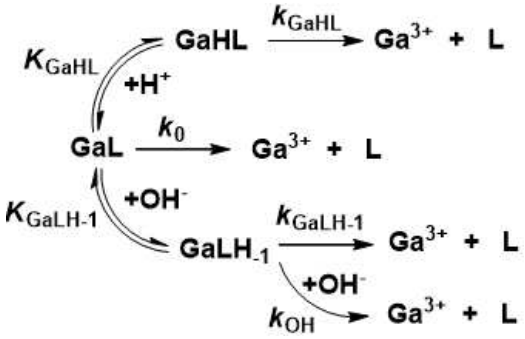

Scheme 1. Dissociation mechanism of [Ga(AAZ2A-exoHB)] and [Ga(AAZ3A-endoHB)]$^-$ complexes.

Labelling of AAZ3A-endoHB and AAZ2A-exoHB with ^{68}Ga(III) isotope

The labelling efficiency of AAZ3A-endoHB and AAZ2A-exoHB with ^{68}Ga was examined at 25 °C and 95 °C, pH 4 and 7 by using 5 min reaction time in the presence of 0.3–100 μM chelator concentration to determine the optimal labelling conditions (Figure 3). Ammonium acetate buffer was used at pH 4 and HEPES buffer at pH 7.

High temperature had no significant effect on the radiolabelling yield of [^{68}Ga(AAZ3A-endoHB)]$^-$ at pH 4. However, the

Table 2. Rate (k) and equilibrium (K) constants and half-life values ($t_{1/2} = \ln 2/k_d$) characterizing the dissociation reactions of the Ga-complexes with AAZ3A-endoHB, AAZ2A-exoHB, PIDAZTA,[29] DATA^m,[46] CyAAZTA[28] and AAZTA[39] (25 °C).

	I	k_1 [$M^{-1}s^{-1}$]	k_{GaLH-1} [s^{-1}]	k_{OH} [$M^{-1}s^{-1}$]	K_{GaHL} [M^{-1}]	$K_{Ga(L)H-1}$ [M^{-1}]	k_d [s^{-1}] (pH = 7.4)	$t_{1/2}$ [h] (pH = 7.4)
AAZ3A-endoHB	0.15 M NaCl	1.2 ± 0.2	$(1.8 \pm 0.2) \times 10^{-4}$	–	1500 ± 600	$(1.0 \pm 0.1) \times 10^{10}$	2.5×10^{-6}	76
AAZ2A-exoHB		–	$(4 \pm 1) \times 10^{-6}$	3.7 ± 0.3	–	2.8×10^6 (pH-pot.)	5.9×10^{-6}	33
PIDAZTA (4aR*, 10aS*)		–	1.4×10^{-4}	–	257	1.1×10^4	7×10^{-4}	0.27
PIDAZTA (4aR*, 10aR*)		–	4.3×10^{-7}	0.6	324	5.6×10^3	6.5×10^{-7}	295
DATA^m		–	8.0×10^{-6}	31	263	1.8×10^6	1.7×10^{-5}	11.2
CyAAZTA	0.1 M KCl	–	1.7×10^{-5}	68	12302	2.0×10^7	2.3×10^{-5}	8.5
AAZTA		–	3.0×10^{-6}	10	1122	5.2×10^4	9.2×10^{-6}	21

$k_1 = k_{GaHL} \times K_{GaHL}$.

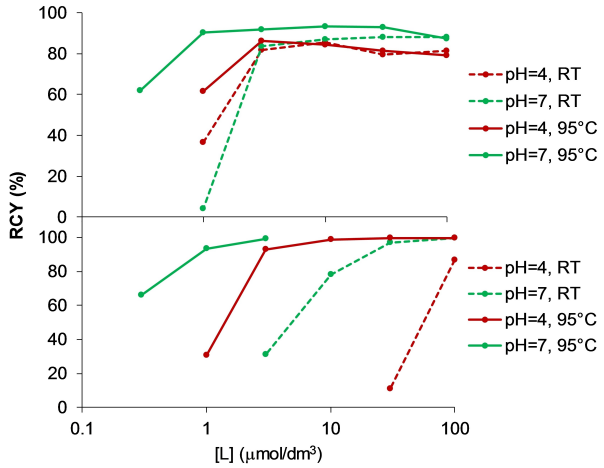

Figure 3. Labelling yield of AAZ3A-endoHB (*top*) and AAZ2A-exoHB (*bottom*) with $^{68}Ga^{3+}$ as a function of ligand concentration (pH 4 or 7; 95 °C or room temperature; 5 min reaction time).

radiochemical yield increased at pH 7 and 95 °C, where five times lower chelator concentration was sufficient to achieve >90% labelling yield (Figure 3, *top*). In the case of [^{68}Ga(AAZ2A-exoHB)] (Figure 3, *bottom*), improved radiolabelling efficiency was observed at high temperature. The radiochemical yields at pH 7 were higher than that at pH 4 at room temperature. The longer reaction time (15 min) had no significant effect on the radiochemical yields of both [^{68}Ga(AAZ3A-endoHB)]$^-$ and [^{68}Ga-(AAZ2A-exoHB)] (Table S2). The optimal labelling conditions for AAZ3A-endoHB and AAZ2A-exoHB with ^{68}Ga (RCY>90%) were found at 95 °C and pH 7 (HEPES buffer) with 5 min reaction time using 1 μM chelator concentration. Labelling efficiency of AAZ2A-exoHB was relatively low at room temperature, while an appropriate radiochemical yield (RCY>80%) was obtained at room temperature and pH 7 using 10 μM chelator in the case of [^{68}Ga(AAZ3A-endoHB)]$^-$.

Synthesis of (AAZ3A-endoHB)-c(RGD) bioconjugate and ^{68}Ga radiolabelling

In view of the better performance of AAZ3A-endoHB in terms of both higher thermodynamic stability and kinetic inertness of the Ga(III) complex and in terms of labelling yield even at room temperature, it was decided to synthesize a bifunctional derivative of this ligand to conjugate it to a cyclic RGD peptide for $\alpha_v\beta_3$-integrin targeting.

The functional group chosen for the conjugation of AAZ3A-endoHB to the *N*-terminus of the peptide was an isothiocyanate that could be inserted on the aromatic ring of the hydroxybenzyl group in *para*-position with respect to the OH-group. Thus, the synthesis of AAZ3A-endoHB-NCS started from previously reported *N,N*-tris(*tert*-butyl acetate)-6-amino-6-methylperhydro-1,4-diazepane **1** (Scheme 2)[33] that was reacted with 2-bromomethyl-4-nitrophenol to introduce the functionalized hydroxybenzyl arm (**2**). The nitro moiety was first converted into an amine by Pd-catalysed hydrogenation (**3**) and then into an isothiocyanate by using thiophosgene (**4**). Final deprotection of the carboxylic groups under acidic conditions (trifluoroacetic acid, TFA) led to the aimed ligand.

The conjugation of AAZ3A-endoHB-NCS to c(RGD) (cyclo(Arg-Gly-Asp-D-Phe-Lys) peptide was accomplished via thiourea bond formation in a mixture of dimethyl sulfoxide (DMSO) and 0.1 M sodium-carbonate buffer (Scheme 3). The final compound was obtained after semi-preparative HPLC purification in good yield. The synthetized conjugate was labelled with ^{68}Ga radioisotope in the following way: the purified cyclotron-produced [^{68}Ga]$GaCl_3$ solution was mixed with NH_4OAc buffer (3 M, pH 4), ascorbic acid (10 mg/mL) and 1 mg/mL aqueous stock solution of the precursor. The labelled compound was purified with solid phase extraction (SPE) using Sep-Pak® Plus light C18 cartridge. The radiochemical purity of the radiotracer was analysed by radio-HPLC (>95%, Figure 4).

The octanol/water partition coefficient (log*P*) of [^{68}Ga-(AAZ3A-endoHB)-c(RGD)] was also determined. The log*P* value was found to be −2.5; thus, the synthetized radiotracer can be considered hydrophilic.

In addition, the stability in human serum of the radio-labelled peptide was determined at 37 °C and it was found perfectly stable for up to 4 h.

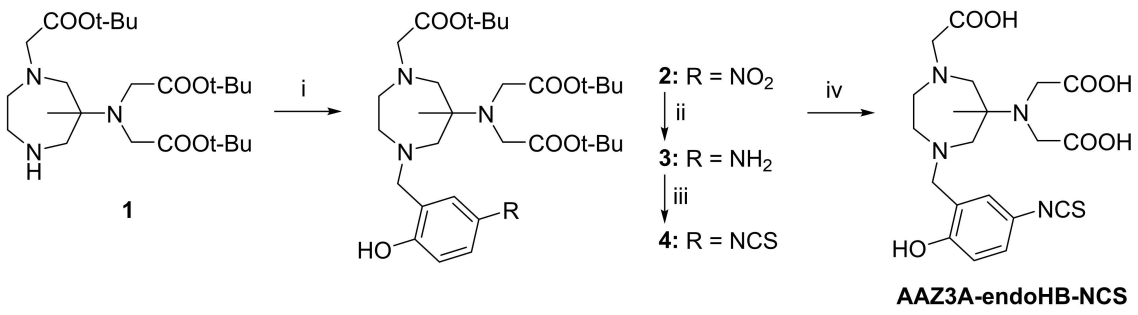

Scheme 2. Synthesis of ligand AAZ3A-endoHB-NCS: i) 2-bromomethyl-4-nitrophenol, K_2CO_3, ACN, rt, on; ii) H_2, 10% Pd/C, MeOH, rt, on; iii) $CSCl_2$, sat. $NaHCO_3$, DCM, 0 °C, 2 h; iv) $(i\text{-Pr})_3SiH$, TFA, rt, 1 h.

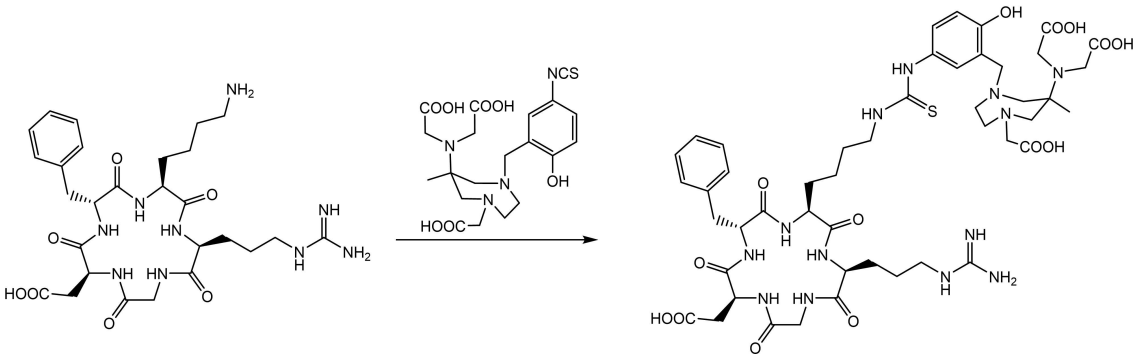

Scheme 3. Synthesis of (AAZ3A-endoHB)-c(RGD) bioconjugate. Reagents and conditions: DMSO-Na_2CO_3 buffer (900 µL, 0.1 M, pH = 9.55).

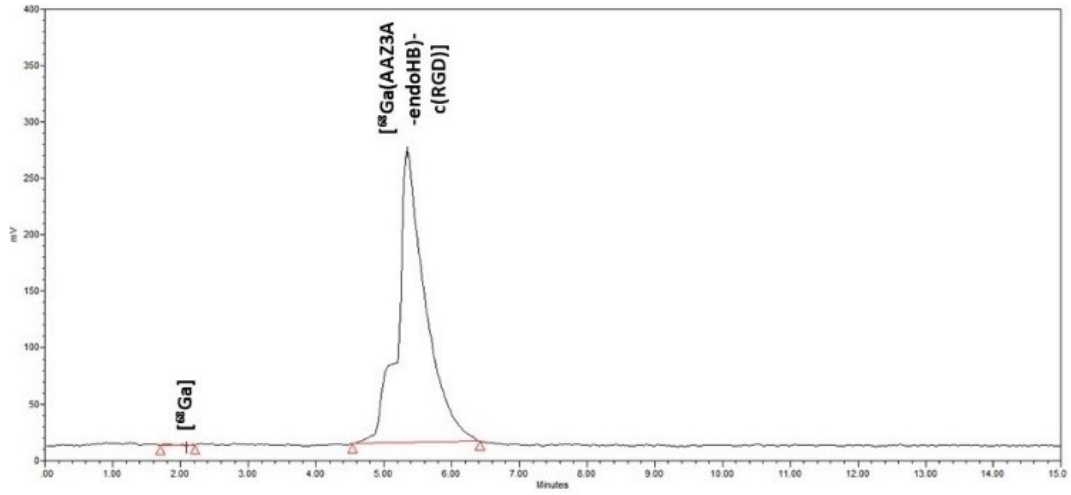

Figure 4. Radio-HPLC chromatogram of the purified [^{68}Ga(AAZ3A-endoHB)-c(RGD)] probe. At 2.1 min there is a minimal fraction of free ^{68}Ga.

In vivo studies

Tumour angiogenesis has an outstanding importance for tumour growth. It determines the rate of proliferation, the effectiveness of anticancer treatment, and plays an important role in the development of distant metastases.[50] In the field of nuclear medicine, there are several radiopharmaceuticals that are specific for one of the characteristic markers (e.g., aminopeptidase N/CD13, VEGF, integrins) of tumour-induced angiogenesis.

One of these potential targets is the $\alpha_v\beta_3$ integrin receptor, which can be detected by radiolabelled RGD (arginine-glycine-asparagine) peptide-based pharmakon's.[51] Thus, the $\alpha_v\beta_3$ integrin receptor targeting efficacy of the [^{68}Ga(AAZ3A-endoHB)-c(RGD)]$^-$ radiopharmaceutical was investigated by in vivo PET imaging 90 min after radiotracer injection using the receptor positive B16-F10 melanoma model.[52] Representative decay-corrected PET images are shown in Figure 5. The subcutaneously growing B16-F10 tumours were clearly identifiable (black arrows, Figure 5) with the Standard Uptake Value (SUV) mean and SUVmax values of 0.36 ± 0.07, and 0.69 ± 0.11, respectively.

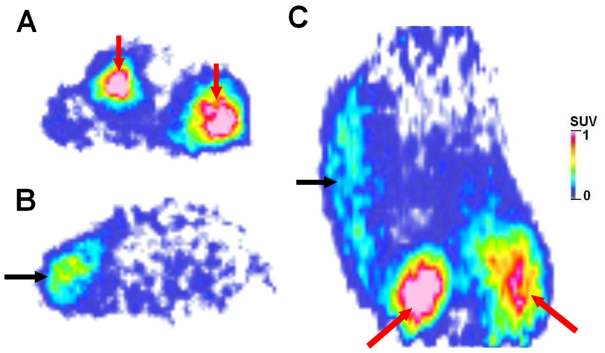

Figure 5. *In vivo* assessment of [^{68}Ga(AAZ3A-endoHB)-c(RGD)] accumulation of B16-F10 melanoma tumours using miniPET imaging. Representative decay-corrected transaxial (A and B) and coronal (C) miniPET image of B16-F10 tumour-bearing C57Bl/6 J mouse 90 min after intravenous injection of [^{68}Ga(AAZ3A-endoHB)-c(RGD)]. PET images were obtained 10 ± 1 days after tumour cell inoculation. Black arrow: B16-F10 tumour, red arrow: kidney.

Conclusion

A detailed thermodynamic and kinetic study on two Ga(III) complexes based on the 6-amino-6-methyl-1,4-diazepine scaf-

fold bearing one 2-hydroxybenzyl pendant arm and two or three acetates, highlighted the advantages of introducing a phenolate donor on the ligand structure. Indeed, a remarkably high thermodynamic stability (up to 6 orders of magnitude higher than $[Ga(AAZTA)]^-$ and $[Ga(DATA^m)]$) and kinetic inertness, ($t_{1/2}$, at pH 7.4, 5.5- and 7-times higher than $[Ga(AAZTA)]^-$ and $[Ga(DATA^m)]$, respectively) was determined for $[Ga(AAZ3A\text{-}endoHB)]^-$. Also [Ga(AAZ2A-exoHB)] showed good stability and kinetic data, although with values lower than those found for $[Ga(AAZ3A\text{-}endoHB)]^-$, except for a much higher structural rigidity as highlighted by ^{1}H NMR data.

A radiolabelling study at different temperatures (25 and 95 °C) and pH (4 and 7) also showed a better performance of the heptadentate AAZ3A-endoHB chelator in terms of labelling yields. Thus, an isothiocyanate bifunctional chelator was synthesized and conjugated to a cyclic RGD peptide for tumour visualization by targeting integrin receptors. Then, the $[^{68}Ga\text{-}(AAZ3A\text{-}endoHB)\text{-}c(RGD)]^-$ conjugate was successfully labelled with ^{68}Ga and then preliminarily tested in vivo on B16-F10 melanoma tumours using miniPET imaging obtaining a good accumulation with SUVmean and SUVmax values of 0.36 ± 0.07, and 0.69 ± 0.11.

Finally, we have shown that phenolate O-donor atoms have better coordination abilities than carboxylates for Ga(III), forming complexes with higher thermodynamic stability and improved kinetic inertness. It is our opinion, though, that the kinetic inertness of the Ga(III) complex can be further improved by enhancing the structural rigidity of the ligand.

Experimental Section

Solution studies on AAZTA-endoHB and AAZ2A-exoHB ligands

Materials: The chemicals used for the experiments were of the highest analytical grade. The concentration of the $CaCl_2$, $ZnCl_2$ and $CuCl_2$ solutions were determined by complexometric titration with standardized Na_2H_2EDTA and xylenol orange ($ZnCl_2$), murexide ($CuCl_2$) and *Patton & Reeder* ($CaCl_2$) as indicators. $Ga(NO_3)_3$ were prepared by dissolving Ga_2O_3 (99.9%, Fluka) in 6 M HNO_3 and evaporating the excess of acid. The solid $Ga(NO_3)_3$ was dissolved in 0.1 M HNO_3 solution. The concentration of the $Ga(NO_3)_3$ solution was determined by using the standardized Na_2H_2EDTA in excess. The excess of the Na_2H_2EDTA was measured with standardized $ZnCl_2$ solution and xylenol orange as indicator. The H^+ concentration of the $Ga(NO_3)_3$ solution was determined by pH potentiometric titration in the presence of Na_2H_2EDTA excess. The concentration of the $H_4AAZ3A\text{-}endoHB$ and $H_3AAZ2A\text{-}exoHB$ was determined by pH-potentiometric titration in the presence and absence of a large (40-fold) excess of $CaCl_2$. The pH-potentiometric titrations were made with standardized 0.2 M NaOH.

Equilibrium measurements: The protonation constants of the ligands, the stability and the protonation constants of Ca(II)- and Zn(II)-complexes formed with AAZ3A-endoHB ligand and the protonation constants of $[Cu(AAZ3A\text{-}endoHB)]^{2-}$, $[Ga(AAZ3A\text{-}endoHB)]^-$ and [Ga(AAZ2A-exoHB)] were determined by pH-potentiometric titration. The metal-to-ligand concentration ratio was 1:1 (the concentration of the ligand was generally 0.002 M). For the pH measurements and titrations, *Metrohm 888 Titrando* titration workstation *Metrohm-6.0234.110* combined electrode was used. Equilibrium measurements were carried out at a constant ionic strength (0.15 M NaCl) in 6 mL samples at 25 °C. The solutions were stirred, and N_2 was bubbled through them. The titrations were made in the pH range of 1.7–12.0. KH-phthalate (pH = 4.005) and borax (pH = 9.177) buffers were used to calibrate the pH meter. For the calculation of $[H^+]$ from the measured pH values, the method proposed by *Irving* et al. was used.[53] A 0.01 M HCl solution was titrated with standardized NaOH solution at 0.15 M NaCl ionic strength. The differences (A) between the measured (pH_{read}) and calculated pH ($-\log[H^+]$) values were used to obtain the equilibrium H^+ concentration from the pH values measured in the titration experiments ($A = 0.04$). For the equilibrium calculations, the stoichiometric water ionic product (pK_w) was also needed to calculate $[OH^-]$ values under basic conditions. The V_{NaOH} – pH_{read} data pairs of the HCl – NaOH titration obtained in the pH range 10.5–12.0 were used to calculate the pK_w value ($pK_w = 13.84$).

NMR experiments: ^{1}H and ^{71}Ga NMR measurement were performed using either a Bruker Avance III (9.4 T) spectrometer, equipped with Bruker Variable Temperature Unit (BVT), Bruker Cooling Unit (BCU) and a BB inverse *z* gradient probe (5 mm). The formation and protonation processes of the $[Ga(AAZ3A\text{-}endoHB)]^-$ and [Ga-(AAZ2A-exoHB)] were followed by ^{1}H and ^{71}Ga NMR spectroscopy at 298 K. For these experiments, 2.25 mM and 2.5 mM aqueous solutions of $[Ga(AAZ3A\text{-}endoHB)]^-$ and [Ga(AAZ2A-exoHB)] in the presence of 0.15 M NaCl were prepared (a capillary with D_2O was used for lock). The pH was adjusted with the addition of the concentrated NaOH and HCl solution. Since the metal exchange of $[Ga(AAZ3A\text{-}endoHB)]^-$ and [Ga(AAZ2A-exoHB)] with $[Ga(OH)_4]^-$ is a slow process on the NMR timescale, the stability constants of $[Ga(AAZ3A\text{-}endoHB)]^-$ and [Ga(AAZ2A-exoHB)] were calculated by using the integrals of the ^{71}Ga NMR signal of $[Ga(OH)_4]^-$ complex. For the calculations of the stability constant, the protonation constant of $[Ga(AAZ3A\text{-}endoHB)]^-$ and [Ga(AAZ2A-exoHB)] obtained by pH-potentiometry and the molar integral values of the ^{71}Ga NMR signal of $[Ga(OH)_4]^-$ complex were used. The molar integral values of the ^{71}Ga NMR signal of $[Ga(OH)_4]^-$ complexes were determined by recording the ^{71}Ga NMR spectra of 0.001, 0.0015, 0.002 and 0.0025 M solutions of $[Ga(OH)_4]^-$ complex (pH = 12.5, 0.1 M NaCl, 25 °C).

Synthesis

Materials and methods for synthesis: All chemicals and solvents were purchased from commercial sources and were used without further purification. Cyclo(Arg-Gly-Asp-D-Phe-Lys) (c(RGD)) was obtained from Caslo AsP (Lyngby, Denmark). Deionized water (18 MΩ cm^{-1}) was produced using a standard Milli-Q system (Millipore, Bedford, MA, USA). NMR spectra (including ^{1}H-decoupled ^{13}C NMR) were recorded on a Bruker Avance III spectrometer operating at 11.74 T, corresponding to a protonic resonance frequency of 499.8 MHz. ^{1}H and ^{13}C NMR chemical shifts are reported relative to TMS and are referenced using the residual proton solvent resonances. ESI mass spectra were recorded on a Waters SQD 3100 or a Waters Acquity UPLC Iclass system (Waters Corporation, Milford, MA, USA). Analytical HPLC-MS were carried out on Waters modular system equipped with Waters 1525 binary pump, Waters 2487 UV/Vis and Waters SQD 3100 (ESCI ionization mode) detectors, using an XBridge™ Phenyl 3.5 μm 4.6×150 mm column (Waters). Semi-preparative HPLC purifications were performed with an XBridge™ Prep Phenyl 5 μm OBD™ 19×100 mm column (Waters).

***1,N,N*-tris(tert-butyl acetate)-4-(2-hydroxy-5-nitrobenzyl)-6-amino-6-methylperhydro-1,4-diazepane (2)**: precursor **1** (0.12 g, 0.26 mmol) was dissolved in ACN (15 mL). K_2CO_3 (0.054 g,

0.39 mmol) was added, followed by a solution of 2-bromomethyl-4-nitrophenol (0.080 g, 0.31 mmol) in ACN (5 mL) and the mixture was stirred at room temperature overnight. After removal of the solvent under reduced pressure, the residue was suspended in EtOAc (40 mL) and washed with H_2O (2×20 mL) and brine (20 mL). The organic phase was dried over anhydrous $MgSO_4$, filtered and evaporated under vacuum. The crude product (0.15 g) was used for the next step without further purification. ESI^+ MS: *m/z* calcd for $[C_{31}H_{50}N_4O_9]^+$: 623.75 $[M+H]^+$; found: 623.62.

***1,N,N*-tris(tert-butyl acetate)-4-(2-hydroxy-5-aminobenzyl)-6-amino-6-methylperhydro-1,4-diazepane (3)**: intermediate **2** (0.15 g, 0.24 mmol) was dissolved in MeOH (20 mL). Raney-Ni (0.015 g) was added and the suspension was stirred under H_2-atmosphere (balloon) at room temperature overnight. After filtration through Celite and evaporation of the filtrate, the amine was obtained in a crude yield of 0.12 g and used directly for the successive conversion. ESI^+ MS: *m/z* calcd for $[C_{19}H_{31}N_3O_2]^+$: 593.77 $[M+H]^+$; found: 593.62.

1,N,N-tris(tert-butyl acetate)-4-(2-hydroxy-5-isothiocyanatobenzyl)-6-amino-6-methylperhydro-1,4-diazepane (4): amine **3** (0.12 g, 0.20 mmol) was dissolved in DCM (5 mL). A saturated water solution of $NaHCO_3$ (5 mL) was added, followed by dropwise addition of a solution of thiophosgene (0.018 mL, 0.24 mmol) in DCM (3 mL) at 0 °C under vigorous stirring, that was continued for 2 h. After evaporation of the volatiles under reduced pressure, the product was purified by semi-preparative HPLC-MS (t_R = 10.5 min, see SI for the method) and obtained as a white powder (0.020 g, 0.031 mmol, 12% with respect to precursor **1**). ^1H NMR (500 MHz, 25 °C, $CDCl_3$), δ (ppm): 7.40 (m, 1H, CH^{Ar}), 7.21 (m, 1H, CH^{Ar}), 7.19 (m, 1H, CH^{Ar}), 4.52 (d, $^2J_{HH}$ = 12.8 Hz, 1H, C<u>H</u>H'Ar), 4.34 (d, $^2J_{HH}$ = 12.8 Hz, 1H, CH<u>H'</u>Ar), 3.5–2.9 (m, 14H, 3xNCH_2CO + NCH_2CH_2N + 2x$NC\underline{H}_2CCH_3$), 1.55 + 1.54 (s, 27H, CH_3^{tBu}), 1.07 (s, 3H, CH_3). ^{13}C NMR (125 MHz, 25 °C, $CDCl_3$), δ (ppm): 173.6 (C=O), 169.1 (C=S), 156.9 ($C^{Ar}OH$), 134.4 ($\underline{C}^{Ar}N$) 130.1 + 129.1 + 118.6 (CH^{Ar}), 116.8 ($\underline{C}^{Ar}CH_2$), 82.8 + 82.4 (C^{tBu}), 65.5 ($N\underline{C}CH_3$), 60.5 (NCH_2Ar), 59.3 ($N\underline{C}H_2CCH_3$), 56.2 ($N\underline{C}H_2CCH_3$), 55.8 ($N\underline{C}H_2CO$), 54.4 ($N\underline{C}H_2CO$), 53.9 ($N\underline{C}H_2CH_2N$), 52.0 ($NCH_2\underline{C}H_2N$), 27.3 (CH_3^{tBu}), 22.1 (CH_3). ESI^+ MS: *m/z* calcd for $[C_{32}H_{51}N_4O_7S]^+$: 635.34 $[M+H]^+$; found: 635.4.

AAZ3A-exoHB-NCS: compound **4** (0.020 g, 0.031 mmol) was dissolved in TFA (1 mL), triisopropylsilane (1 drop) was added and the mixture was stirred at room temperature for 1 h. The solvent was evaporated under reduced pressure and the product was purified by semi-preparative HPLC-MS (t_R = 5.2 min, see Si for the method) and obtained as a white solid (5 mg, trifluoroacetate salt, 43%). ^1H NMR (500 MHz, 25 °C, D_2O), δ (ppm): 7.37 (m, 2H, 2xCH^{Ar}), 6.94 (m, 1H, CH^{Ar}), 4.36 (d, $^2J_{HH}$ = 13.1 Hz, 1H, C<u>H</u>H'Ar), 4.32 (d, $^2J_{HH}$ = 13.1 Hz, 1H, CH<u>H'</u>Ar), 3.87 (m, 2H, NCH_2CO), 3.7–3.3 (m, 12H, 2xNCH_2CO + NCH_2CH_2N + 2x$NC\underline{H}_2CCH_3$), 1.12 (s, 3H, CH_3). ^{13}C NMR (125 MHz, 25 °C, D_2O), δ (ppm): 174.3 (C=O), 172.7 (C=O), 162.3 (C=S), 155.7 ($C^{Ar}OH$), 133.1 ($\underline{C}^{Ar}N$) 132.3 + 120.9 + 116.1 (CH^{Ar}), 115.6 ($\underline{C}^{Ar}CH_2$), 62.8 ($N\underline{C}CH_3$), 58.4 (NCH_2Ar), 58.3 ($N\underline{C}H_2CCH_3$), 58.0 ($N\underline{C}H_2CCH_3$), 57.3 ($N\underline{C}H_2CO$), 54.1 ($N\underline{C}H_2CO$), 51.7 ($N\underline{C}H_2CH_2N$), 49.7 ($NCH_2\underline{C}H_2N$), 17.4 (CH_3). ESI^+ MS: *m/z* calcd for $[C_{20}H_{27}N_4O_7]^+$: 467.16 $[M+H]^+$; found: 467.4.

(AAZ3A-endoHB)-c(RGD): to a solution of cyclo(Arg-Gly-Asp-D-Phe-Lys) (5 mg, 0.0083 mmol) in Na_2CO_3 buffer (900 µL, 0.1 M, pH 9.55) was added the solution of compound AAZ3A-endoHB-NCS (0.0107 mmol) in DMSO (100 µL). The reaction mixture was stirred overnight at room temperature and then diluted with water, frozen, and lyophilized. The crude product was purified by semipreparative RP-HPLC. For semipreparative RP-HPLC, the following conditions were used: solvent A: 0.1% HCOOH solvent, B: 95% acetonitrile, gradient: 0 min: 100% A, 2 min: 100% A, 32 min: 100% B, 40 min 100% B. The product was collected between 12.9 and 13.2 min. The product solution was frozen, lyophilized to give (AAZ3A-endoHB)-c(RGD) (1.3 mg, 15.4%). HRMS (ESI): *m/z* calcd for $[C_{47}H_{67}N_{13}O_{14}S]^+$: 1070.4729 $[M+H]^+$ and 535.7404 $[M+2H^+]/2$; found: 1070.4691 $[M+H]^+$, 535.7371 $[M+2H^+]/2$.

Radiochemistry: ^{68}Ga radionuclide was obtained from a $^{68}Ge/^{68}Ga$ isotope generator (Eckert-Ziegler, GalliaPharm®, Berlin, Germany, eluent: 0.1 M u.p. HCl) and by cyclotron production from the irradiation of solid enriched ^{68}Zn with 12 MeV proton beam on a GE PETtrace cyclotron. Activity measurements were implemented by CAPINTEC CRC-15PET dose calibrator and a Perkin Elmer Packard Cobra gamma counter (Llantrisant, UK). Semipreparative RP HPLC and analytical radio-HPLC were carried out using Waters LC Module 1 HPLC and Waters 2695 Alliance HPLC system, connected to a UV detector and an ATOMKI 120 CsI scintillation detector. Semi-preparative RP-HPLC was performed using a Luna C18 10 µm (250×10 mm) column. Analytical HPLC was performed using a Kinetex XB-C18 2.6 µm 100 Å (50×4.60 mm) column, solvent A: TFA (0.05 M); solvent B: 95% acetonitrile. Purification of radiolabelled compound was carried out with a Sep-Pak® Plus light C18 cartridge. 100 µL of the purified $[^{68}Ga]GaCl_3$ solution (~77 MBq) was transferred into an Eppendorf vial and mixed with 300 µL of NH_4OAc buffer (3 M, pH 4), 5.5 µL ascorbic acid (10 mg/mL), and 30 µL of an aqueous stock solution of (AAZ3A-endoHB)-c(RGD) bioconjugate (1 mg/mL). The reaction was carried out at 95 °C for 15 min. Then the reaction mixture was passed through a pre-conditioned (5 mL 96% EtOH, 10 mL water) reversed-phase C18 SPE cartridge (Sep-Pak® Plus light C18, Waters). After washing the cartridge with 1 mL water, the radiolabelled product was eluted with 200 µL 96% EtOH, concentrated, and resolved with 200 µL saline. The purified radiolabelled complex was analysed by radio-HPLC on Waters Alliance 2695 HPLC system with Kinetex 2.6 µm XB-C18 100 Å (50×4.60 mm) column. Solvent A 0.05% TFA, solvent B: 95% ACN, gradient: 0 min: 100% A, 1 min: 100% A, 10 min: 100% B, 11 min: 100% B, 12 min: 100% A. The molar activity was 1.07 ± 0.3 GBq/µmol.

Determination of log*P* Value of [^{68}Ga]Ga-AAZTA-cRGD: A volume of 50 µL of the purified [^{68}Ga]Ga-AAZTA-cRGD solution (approx. 2–3 MBq) was mixed with 450 µL of water and 500 µL of 1-octanol in an Eppendorf vial. The mixture was shaken with a vortex shaker for 5 min and centrifuged (9000 rpm) for 5 min. 3×20 µL portions from the two solvents were pipetted into a vial. The radioactivity of the fractions was determined with a gamma counter.

Stability of [^{68}Ga(AAZ3A-endoHB)-c(RGD)]$^-$ in human serum: 50 µL of ^{68}Ga-AAZ3A-endoHB-RGD was diluted to 500 µL with human serum and incubated at 37 °C in a closed syringe to prevent acidification caused by CO_2. Samples were analyzed by UPLC-UV-RA at 30 min, 60 h and 120 h. Analytical conditions: sample-preparation: 10 µL of samples were diluted to 50 µL with H_2O, column: XBridge Premier Protein, SEC, 250 A, 2.5 µm, 4.6×150 mm column, eluent: A: 100 mM pH = 7.2 NH_4OAc, flow: 0.45 mL/min, isocratic, delay between UV and RA: 0.2 min.

In vivo studies of [^{68}Ga(AAZ3A-endoHB)-c(RGD)]$^-$ bioconjugate

***In vivo* tumour model**: C57BL/6 J mice (12-week-old, female, n = 5) were housed under standard conditions (26 ± 2 °C, 55 ± 10% humidity, and artificial lighting with 12–12 h). Semi-synthetic rodent chow (Akronom Ltd., Budapest, Hungary) and drinking water were available *ad libitum* to all the experimental animals. Laboratory animals were kept and treated in compliance with all applicable sections of the Hungarian Laws and regulations of the European Union (permission number: 21/2017/DEMÁB). For the induction of $\alpha_v\beta_3$ integrin receptor positive melanoma tumors

C57BL/6 J mice were injected with 1×10^6 B16-F10 tumor cells in 100 μL saline subcutaneously into the left shoulder area. *In vivo* PET imaging was carried out 10 ± 1 days after tumor cell inoculation at the tumor volume of 115 ± 15 mm^3.

***In vivo* PET imaging**: For in vivo imaging studies B16-F10 tumor-bearing mice were injected intravenously with 9.25 ± 0.31 MBq of [^{68}Ga(AAZ3A-endoHB)-c(RGD)]$^-$ via the lateral tail vein, and PET scans were performed under 1.5% isoflurane (Forane, AbbVie) anesthesia (Tec3 Isoflurane Vaporizer, Eickemeyer Veterinary Equipment, UK) using the preclinical MiniPET-II imaging device (University of Debrecen, Faculty of Medicine, Department of Medical Imaging, Division of Nuclear Medicine and Translational Imaging). Reconstructed images were analyzed using the BrainCad software image analysis software. Radiotracer uptake was expressed in terms of standardized uptake values (SUVs). SUV was calculated as follows: SUV = [VOI activity (Bq/mL)]/[injected activity (Bq)/animal weight (g)], assuming a density of 1 g/mL.

Acknowledgements

L. T. acknowledges the financial support from Università del Piemonte Orientale (Ricerca locale 2019). Open Access funding provided by Università degli Studi del Piemonte Orientale Amedeo Avogadro within the CRUI-CARE Agreement.

Conflict of Interest

The authors declare no conflict of interest.

Data Availability Statement

The data that support the findings of this study are available from the corresponding author upon reasonable request.

Keywords: gallium · imaging agents · $\alpha_v\beta_3$ integrin targeting · ligand design · PET · radiopharmaceuticals

[1] T. Shen, R. Weissleder, M. Papisov, A. Bogdanov, T. J. Brady, *Magn. Reson. Med.* **1993**, *29*, 599–604.
[2] L. Russelli, J. Martinelli, F. De Rose, S. Reder, M. Herz, M. Schwaiger, W. Weber, L. Tei, C. D'Alessandria, *ChemMedChem* **2020**, *15*, 284–292.
[3] S. J. Archibald, L. Allott, *EJNMMI Radiopharm. Chem.* **2021**, *6*, 32.
[4] M. Brandt, J. Cardinale, M. L. Aulsebrook, G. Gasser, T. L. Mindt, *J. Nucl. Med.* **2018**, *59*, 1500–1506.
[5] M. Vorster, A. Maes, C. Van de Wiele, M. Sathekge, *Semin. Nucl. Med.* **2016**, *46*, 436–447.
[6] I. Velikyan, *Theranostics* **2014**, *4*, 47–80.
[7] I. Velikyan, *J. Labelled Compd. Radiopharm.* **2015**, *58*, 99–121.
[8] S. Ray Banerjee, Z. Chen, M. Pullambhatla, A. Lisok, J. Chen, R. C. Mease, M. G. Pomper, *Bioconjugate Chem.* **2016**, *27*, 1447–1455.
[9] T. Maurer, M. Eiber, M. Schwaiger, J. E. Gschwend, *Nat. Rev. Urol.* **2016**, *13*, 226–235.
[10] M. Fani, L. Del Pozzo, K. Abiraj, R. Mansi, M. L. Tamma, R. Cescato, B. Waser, W. A. Weber, J. C. Reubi, H. R. Maecke, *J. Nucl. Med.* **2011**, *52*, 1110–1118.
[11] R. Eychenne, C. Bouvry, M. Bourgeois, P. Loyer, E. Benoist, N. Lepareur, *Molecules* **2020**, *25*, 4012.
[12] B. P. Burke, G. S. Clemente, S. J. Archibald, *J. Labelled Compd. Radiopharm.* **2014**, *57*, 239–243.
[13] T. W. Price, J. Greenman, G. J. Stasiuk, *Dalton Trans.* **2016**, *45*, 15702–15724.
[14] M. Eder, B. Wangler, S. Knackmuss, F. LeGall, M. Little, U. Haberkorn, W. Mier, M. Eisenhut, *Eur. J. Nucl. Med. Mol. Imaging* **2008**, *35*, 1878–1886.
[15] C. F. Ramogida, J. F. Cawthray, E. Boros, C. L. Ferreira, B. O. Patrick, M. J. Adam, C. Orvig, *Inorg. Chem.* **2015**, *54*, 2017–2031.
[16] A. J. Smith, P. J. Gawne, M. T. Ma, P. J. Blower, R. Southworth, N. J. Long, *Dalton Trans.* **2018**, *47*, 15448–15457.
[17] A. J. Smith, B. E. Osborne, G. P. Keeling, P. J. Blower, R. Southworth, N. J. Long, *Dalton Trans.* **2020**, *49*, 1097–1106.
[18] C. L. Ferreira, D. T. T. Yapp, D. Mandel, R. K. Gill, E. Boros, M. Q. Wong, P. Jurek, G. E. Kiefer, *Bioconjugate Chem.* **2012**, *23*, 2239–2246.
[19] I. Velikyan, H. Maecke, B. Langstrom, *Bioconjugate Chem.* **2008**, *19*, 569–573.
[20] B. P. Waldron, D. Parker, C. Burchardt, D. S. Yufit, M. Zimny, F. Roesch, *Chem. Commun.* **2013**, *49*, 579–581.
[21] C. Fersing, N. Masurier, L. Rubira, E. Deshayes, V. Lisowski, *Pharmaceuticals* **2022**, *15*, 234.
[22] F. Travagin, L. Lattuada, G. B. Giovenzana, *Coord. Chem. Rev.* **2021**, *438*, 213908.
[23] J. P. Sinnes, U. Bauder-Wüst, M. Schäfer, E. S. Moon, K. Kopka, F. Rösch, *EJNMMI Radiopharm. Chem.* **2020**, *5*, 28.
[24] L. Greifenstein, T. Grus, J. Nagel, J. P. Sinnes, F. Rosch, *Appl. Radiat. Isot.* **2020**, *156*, 108867.
[25] L. Manzoni, L. Belvisi, D. Arosio, M. P. Bartolomeo, A. Bianchi, C. Brioschi, F. Buonsanti, C. Cabella, C. Casagrande, M. Civera, M. De Matteo, L. Fugazza, L. Lattuada, F. Maisano, L. Miragoli, C. Neira, M. Pilkington-Miksa, C. Scolastico, *ChemMedChem* **2012**, *7*, 1084–1093.
[26] J. Pfister, D. Summer, C. Rangger, M. Petrik, E. von Guggenberg, P. Minazzi, G. B. Giovenzana, L. Aloj, C. Decristoforo, *EJNMMI Res.* **2015**, *5*, 74.
[27] A. Vagner, E. Gianolio, S. Aime, A. Maiocchi, I. Toth, Z. Baranyai, L. Tei, *Chem. Commun.* **2016**, *52*, 11235–11238.
[28] A. Vagner, C. D'Alessandria, G. Gambino, M. Schwaiger, S. Aime, A. Maiocchi, I. Toth, Z. Baranyai, L. Tei, *ChemistrySelect* **2016**, *1*, 163–171.
[29] E. Farkas, A. Vagner, R. Negri, L. Lattuada, I. Toth, V. Colombo, D. Esteban-Gomez, C. Platas-Iglesias, J. Notni, Z. Baranyai, G. B. Giovenzana, *Chem. Eur. J.* **2019**, *25*, 10698–10709.
[30] H. Lahnif, T. Grus, S. Pektor, L. Greifenstein, M. Schreckenberger, F. Rosch, *Molecules* **2021**, *26*, 6332.
[31] E. S. Moon, F. Elvas, G. Vliegen, S. De Lombaerde, C. Vangestel, S. De Bruycker, A. Bracke, E. Eppard, L. Greifenstein, B. Klasen, V. Kramer, S. Staelens, I. De Meester, P. Van der Veken, F. Rosch, *EJNMMI Radiopharm. Chem.* **2020**, *5*, 19.
[32] J. Martinelli, M. Boccalon, D. Horvath, D. Esteban-Gomez, C. Platas-Iglesias, Z. Baranyai, L. Tei, *Inorg. Chem. Front.* **2022**, *9*, 2271–2283.
[33] J. Martinelli, D. Remotti, L. Tei, *Org. Biomol. Chem.* **2020**, *18*, 5245–5252.
[34] J. Greiser, C. Kuhnel, H. Gorls, W. Weigand, M. Freesmeyer, *Dalton Trans.* **2018**, *47*, 9000–9007.
[35] Y. M. Hsiao, C. J. Mathias, S. P. Wey, P. E. Fanwick, M. A. Green, *Nucl. Med. Biol.* **2009**, *36*, 39–45.
[36] O. Thews, W. Dillenburg, M. Fellner, H. G. Buchholz, N. Bausbacher, M. Schreckenberger, F. Rosch, *Eur. J. Nucl. Med. Mol. Imaging* **2010**, *37*, 1935–1942.
[37] F. Mendes, A. Paulo, I. Santos, *Dalton Trans.* **2011**, *40*, 5377–5393.
[38] F. Silva, M. P. C. Campello, L. Gano, C. Fernandes, I. C. Santos, I. Santos, J. R. Ascenso, M. J. Ferreira, A. Paulo, *Dalton Trans.* **2015**, *44*, 3342–3355.
[39] Z. Baranyai, F. Uggeri, A. Maiocchi, G. B. Giovenzana, C. Cavallotti, A. Takacs, I. Toth, I. Banyai, A. Benyei, E. Brucher, S. Aime, *Eur. J. Inorg. Chem.* **2013**, *2013*, 147–162.
[40] V. Kubicek, J. Havlickova, J. Kotek, T. Gyula, P. Hermann, E. Toth, I. Lukes, *Inorg. Chem.* **2010**, *49*, 10960–10969.
[41] Z. Baranyai, G. Tircso, F. Rosch, *Eur. J. Inorg. Chem.* **2020**, *2020*, 36–56.
[42] S. Pandey, in *Met. Ions Bio-Imaging Tech.* (Ed.: R. Sigel, A.; Freisinger, E; Sigel), De Gruyter, Berlin, **n.d.**, pp. 315–346.
[43] R. J. Motekaitis, A. E. Martell, *Inorg. Chem.* **1980**, *19*, 1646–1651.
[44] R. Delgado, Y. Sun, R. J. Motekaitis, A. E. Martell, *Inorg. Chem.* **1993**, *32*, 3320–3326.
[45] C. F. G. C. Geraldes, R. Delgado, A. M. Urbano, J. Costa, F. Jasanada, F. Nepveu, *J. Chem. Soc., Dalton Trans.* **1995**, 327–335.
[46] E. Farkas, J. Nagel, B. P. Waldron, D. Parker, I. Toth, E. Brucher, F. Rosch, Z. Baranyai, *Chem. Eur. J.* **2017**, *23*, 10358–10371.
[47] C. J. Broan, J. P. L. Cox, A. S. Craig, R. Kataky, D. Parker, A. Harrison, A. M. Randall, G. Ferguson, *J. Chem. Soc. Perkin Trans. 2* **1991**, 87–99.

[48] S. Hajela, M. Botta, S. Giraudo, J. Xu, K. N. Raymond, S. Aime, *J. Am. Chem. Soc.* **2000**, *122*, 11228–11229.
[49] J. Simecek, M. Schulz, J. Notni, J. Plutnar, V. Kubicek, J. Havlickova, P. Hermann, *Inorg. Chem.* **2012**, *51*, 577–590.
[50] D. R. Bielenberg, B. R. Zetter, *Cancer J.* **2015**, *21*, 267–273.
[51] C. Liolios, C. Sachpekidis, A. Kolocouris, A. Dimitrakopoulou-Strauss, P. Bouziotis, *Molecules* **2021**, *26*, 1792.
[52] S. Yacobovich, L. Tuchinsky, M. Kirby, T. Kardash, O. Agranyoni, E. Nesher, B. Redko, G. Gellerman, D. Tobi, K. Gurova, I. Koman, O. A. Fabian, A. Pinhasov, *Oncotarget* **2016**, *7*, 63549–63560.
[53] H. M. Irving, M. G. Miles, L. D. Pettit, *Anal. Chim. Acta* **1967**, *38*, 475–488.

Manuscript received: December 5, 2022
Accepted manuscript online: January 31, 2023
Version of record online: ■■, ■■

AAZTA- and DATA-like ligands bearing one phenolate pendant arm form Ga(III) complexes with significant thermodynamic stability and kinetic inertness. ^{68}Ga labelling was efficient both at room temperature and at 95 °C and an $\alpha_v\beta_3$ integrin targeting probe was synthesized, labelled, and tested in vivo on B16-F10 tumours.

Dr. J. Martinelli, L. M. Zapelli, Dr. M. Boccalon, Dr. A. Vágner, Dr. G. Nagy, Dr. A. Fekete, Dr. D. Szikra, Dr. G. Trencsényi, Dr. Z. Baranyai, Prof. Dr. L. Tei**

1 – 12

AAZTA-Like Ligands Bearing Phenolate Arms as Efficient Chelators for ^{68}Ga Labelling in vitro and in vivo